Journal of Hazardous Materials 176 (2010) 451–458

Contents lists available at ScienceDirect

Journal of Hazardous Materials

journal homepage: www.elsevier.com/locate/jhazmat

# Preparation and characterization of tungsten-loaded titanium dioxide photocatalyst for enhanced dye degradation

Saepurahman, M.A. Abdullah*, F.K. Chong

*Department of Chemical Engineering, Universiti Teknologi Petronas, Bandar Seri Iskandar, 31750 Tronoh, Perak D.R., Malaysia*

ARTICLE INFO

*Article history:*
Received 23 July 2009
Received in revised form 15 October 2009
Accepted 7 November 2009
Available online 13 November 2009

*Keywords:*
Photocatalysis
Titanium dioxide
Tungsten loading
Methylene blue
Environmental remediation

ABSTRACT

Tungsten-loaded $TiO_2$ photocatalyst has been successfully prepared and characterized. TEM analysis showed that the photocatalysts were nanosize with the tungsten species forming layers of coverage on the surface of $TiO_2$, but not in clustered form. This was confirmed by XRD and FT-Raman analyses where tungsten species were well dispersed at lower loading (<6.5 mol%), but were in crystalline $WO_3$ at higher loadings (>12 mol%). In addition, loading with tungsten could stabilize the anatase phase from transforming into inactive rutile phase and did not shift the optical absorption to the visible region as shown by DRUV–vis analysis. PZC value of $TiO_2$ was found at 6.4, but the presence of tungsten at 6.5 mol% $WO_3$, decreased the PZC value to 3. Tungsten-loaded $TiO_2$ was superior to unmodified $TiO_2$ with 2-fold increase in degradation rate of methylene blue, and equally effective for the degradation of different class of dyes such as methyl violet and methyl orange at 1 mol% $WO_3$ loading.



## 1. Introduction

The presence of colour and its causative compound is undesirable for domestic or industrial uses as colour is visible and can be an indication of pollution [1]. WHO guidelines for drinking water quality, has set the maximum value for permissible colour at 15–20 units [2]. Several new technologies in wastewater decolourization have emerged with improved performance and more environmentally friendly. These include Advanced Oxidation Processes (AOPs) such as heterogeneous photocatalysis, Fenton and Photo-Fenton, and ozonation which have received considerable attention due to their compliance with Green Chemistry concept in promoting innovative technologies that reduce or eliminate the use or generation of hazardous substances in the design, manufacturing and use of chemical products [3]. Heterogeneous photocatalysis especially has several advantages, as it uses no reagent. The only chemical used, metal oxide photocatalyst such as titanium dioxide ($TiO_2$) is abundant and harmless. However, $TiO_2$ photocatalysis lacks efficiency due to the high rate of recombination of electrons and holes [4]. In addition, due to its large bandgap energy, $E_g$ of 3.0–3.2 eV, it can only be activated by UV light, which accounts only 3–4% of sunlight spectrum [5]. Efforts have been made using chemical or physical methods, to enhance the photocatalytic activity of $TiO_2$ through modification with different group of metals such as alkaline metals [6], earth alkaline metals [7], transition metals [8], rare earth metals [9], and noble metals [10], but with varying degree of results.

$TiO_2$ has three natural phases—anatase, rutile, and brookite. Modification with certain metals such as Ni [11], Fe [11,12], Th [12], Cu [12], V and Mo [13], Co [14], Sn [15], and Ag [16], may alter the phase transformation of $TiO_2$ from active anatase to inactive rutile by lowering the activation energy. The activation energy is further affected by metal dosage and method of preparation. On the other hand, metals such as Mg and Ba [17], Mn [18], Tb, Eu and Sm [19], La [20], and Sc and Nb [21] have been reported to inhibit phase transformation.

Degradation of pollutant can be influenced by both intrinsic and extrinsic factors. Intrinsic factors include the nature of the photocatalyst itself such as crystallinity, surface area, morphology, and optical absorption. Extrinsic factors are the process parameters that affect the photodegradation rate such as dye concentration, catalyst loading, pH, light wavelength and intensity, temperature, and oxygen pressure [22–24]. In addition, the presence of oxidants and dissolved metal ions and organic materials also affect the degradation rates [24]. From both application and economic point of view for operational effectiveness of a photocatalyst, the effects of extrinsic factors are important to be determined particularly the optimum decolourization conditions and limitations.

The objective of this study was to evaluate the effect of $TiO_2$ modification with tungsten trioxide, $WO_3$, using impregnation method, on the photocatalytic activity. Characterization of the photocatalyst was carried out using transmission electron microscopy (TEM), X-ray diffraction (XRD), Fourier transform Raman (FT-Raman), diffuse reflectance ultraviolet visible spec-

* Corresponding author. Tel.: +60 5 3687636; fax: +60 5 3656176.
*E-mail address:* azmuddin@petronas.com.my (M.A. Abdullah).

0304-3894/$ – see front matter © 2009 Elsevier B.V. All rights reserved.
doi:10.1016/j.jhazmat.2009.11.050

troscopy (DRUV-Vis) and point of zero charge (PZC) methods to understand the physico-chemical properties of the photocatalyst. The photocatalytic activity was tested against the decolourization of methylene blue (MB), methyl violet (MV), and methyl orange (MO) as model dyes in wastewater streams. The effects of process parameters such as initial dye concentration, catalyst loading, and initial pH were investigated.

## 2. Materials and methods

### 2.1. Chemicals

$TiO_2$ P25 was purchased from Evonik Degussa (Germany) while ammonium metatungstate (AMT) was from Fluka (Germany). Dyes used in the experiment such as methylene blue and methyl orange were from Merck (Germany), while methyl violet was from Acros Organics (USA).

### 2.2. Preparation

The photocatalyst $TiO_2$ P25 was weighed and dispersed in distilled water and an appropriate amount of aqueous solution of AMT solution was added to provide the required tungsten trioxide ($WO_3$) loading. The suspension was stirred overnight to equilibrate the adsorption–desorption processes. The suspension was dried overnight in an oven at 120 °C. The powder was grounded using mortar and pestle, followed by calcination at different temperatures and duration, using a programmable furnace (Nabertherm, Germany) at a ramp rate of 3.5 °C/min under static air. The powder was subsequently sieved prior to characterization and decolourization studies. The photocatalyst was marked based on tungsten loading, calcination temperature and calcination duration. For example, 1-w-450-2 represents 1 mol% $WO_3$ loading and calcination at 450 °C for 2 h.

### 2.3. Characterization

Phases present in the photocatalysts were determined by powder X-ray diffraction (XRD) method. Diffraction pattern was recorded on Bruker D8 Advance XRD (Germany), equipped with Cu Kα = 1.5406 Å, at 60 kV and 80 mA. The pattern was scanned from $2\theta = 2–80^\circ$ at scan rate of 2°/min. Diffractogram was aligned with the International Centre for Diffraction Data (ICDD) database. The anatase fraction, $F_A$, of the photocatalyst was determined using Eq. (1), where $I_A$ and $I_R$ are intensities of anatase and rutile peak at (1 0 1) and (1 1 0) plane, respectively [25]:

$$F_A = \frac{0.79 I_A}{079 I_A + I_R} \quad (1)$$

FT-Raman analysis was carried out to identify surface species present in the photocatalyst. The analysis was carried out using Horiba Jobin Yvon HR 800 (USA), equipped with a laser at λ = 514.532 nm with CCD-5984 detector. The spectrum was recorded from 200 to 1200 nm.

TEM analysis was carried out to obtain more information about the morphology of the photocatalysts. Analysis was carried out using Philips CM12 TEM (The Netherlands), operated at 80 kV. Sample was placed on a grid prior to analysis. In order to produce comparable photomicrographs, samples were magnified to the same magnification level.

Optical absorption of the photocatalyst was determined using DRUV–vis spectrophotometer. Analysis was performed using Shimadzu UV3150 Spectrometer (Japan), equipped with integrating sphere. The spectrum was recorded between 220 and 800 nm at 20 nm interval. Barium sulfate was used as a standard white.

Point zero of charge is defined as the pH at which the net charge is zero. In our study, PZC was determined by mass titration method [26]. A weighted amount of catalyst was mixed with distilled water to give concentrations of 0.1, 1, 5, 10, and 20% (w/v). The suspensions were stirred for 24 h to equilibrate the adsorption–desorption processes, after which pH of the suspensions was determined using a pH meter (Mettler Toledo, USA). PZC value was taken at the point where further addition of solids did not produce any significant pH change.

### 2.4. Photodegradation studies

The prepared tungsten-loaded $TiO_2$ was weighed and mixed with 10 mL of distilled water in a glass dish. The suspension was ultra-sonicated for 10 min using ultra-sonicator (Barnstead, USA), followed by addition of MB solution to give a final concentration of 40 ppm, volume 100 mL, and catalyst loading 1 g/L. The dish was covered with a watch glass and left to ambient temperature at 26–29 °C. Initial pH of the solution was 6. The suspension was kept in the dark and continuously stirred using a magnetic stirrer (Ika, Germany) to equilibrate the adsorption–desorption processes. After 4 h in the dark, the dish was illuminated with a 250 W metal halide lamp (Venture Lighting, USA), providing the light intensity of 21,000 lx at a distance of 5 cm from the top of the watch glass. Five hundred microliter of the suspension was taken at fixed interval where it was centrifuged twice at 2000 × *g* (Sigma, USA) to remove any particulate. The concentrations of MB in the suspension were then determined using Shimadzu 3150 UV–vis spectrophotometer (Japan) at λ = 664.50 nm. The concentrations of MV and MO were determined at wavelength 583.5 and 464 nm, respectively. The photocatalytic degradation of MB was approximated into first-order kinetics as shown in Eq. (2) [24]:

$$\ln \frac{[MB]_t}{[MB]_e} = -k_1 t \quad (2)$$

where $[MB]_t$ and $[MB]_e$ are the concentration of MB at $t$ time and equilibrium, respectively, while $k_1$ is the first-order reaction rate constant.

## 3. Results and discussion

### 3.1. Preparation and characterization

#### 3.1.1. TEM and spectral analyses

The photocatalyst $TiO_2$ is normally white in colour, while the typical colour of $WO_3$ is yellow. Upon calcinations, the tungsten-loaded $TiO_2$ photocatalyst turned pale yellow with a tinge of bluish colour. The bluish colour became more intense when tungsten loading was increased. As shown by the TEM micrograph (Fig. 1), the particles tend to stick-to-each other forming bigger particles with increasing $WO_3$ loading and also with increasing calcinations temperatures. Based on XRD, tungsten trioxide ($WO_3$) phases only emerged at high tungsten loading of 12 mol% $WO_3$ (Fig. 2). There was also no new peak that could be ascribed to the solid solution of $W_xTi_{1-x}O_2$. The absence of the $WO_3$ phase at or below 6.5 mol% suggests that $WO_3$ was well dispersed on the $TiO_2$ surface as an amorphous layer. Additionally, it could be beyond the threshold of the XRD sensitivity for detection [28] or the crystalline phase of $WO_3$ can only be detected if the loading exceeds the dispersion capacity on $TiO_2$ as discussed further later. In a study on thermal decomposition of AMT [27], the blue colour is attributed to the traces of $W_{20}O_{58}$ produced from partial reduction of $WO_3$ by ammonia, in which the latter being liberated during the decomposition of AMT. Observation on flame-made $WO_3/TiO_2$ has suggested that the blue colour is due to the presence of $W^{6+}$ and $W^{5+}$ at equilibrium [28].

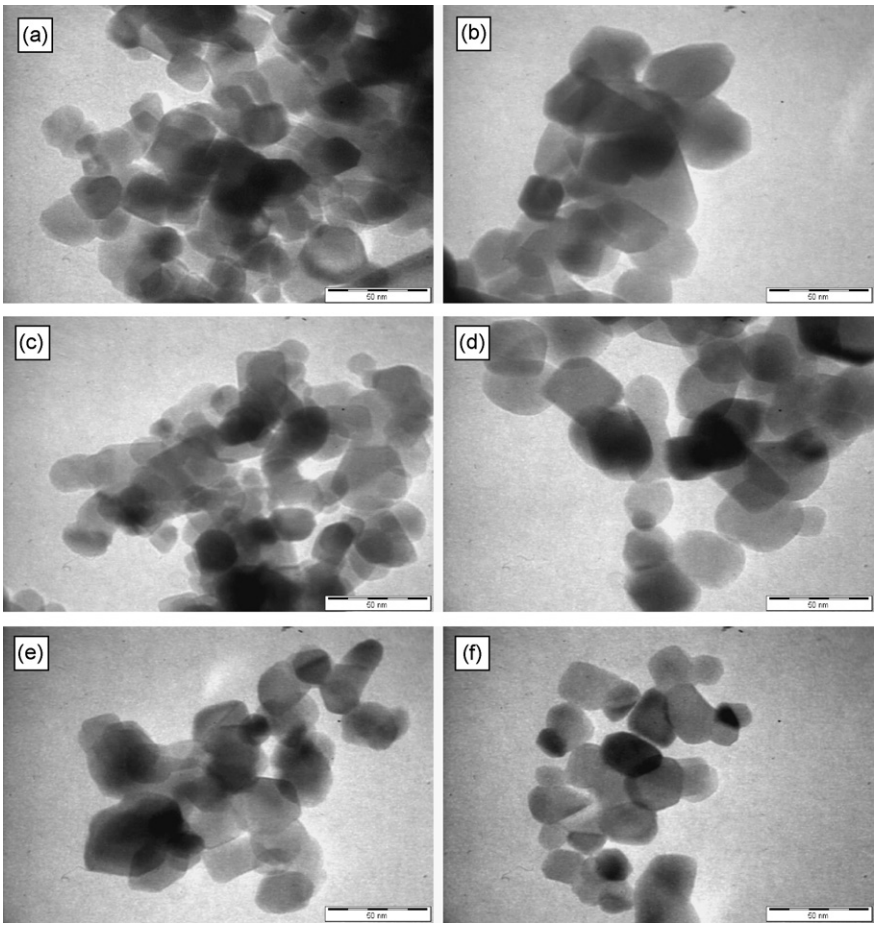


**Fig. 1.** TEM micrograph of $TiO_2$ at different tungsten loadings and calcinations temperatures: (a) 0-w-450-2, (b) 0-w-650-2, (c) 1-w-450-2, (d) 1-w-650-2, (e) 6.5-w-450-2, and (f) 6.5-w-650-2.

The Raman spectrum (Fig. 3) of unmodified P25 showed three intense peaks at 399, 519, and 639 $cm^{-1}$ which can be attributed to the anatase phase [29,30]. A broad and weak peak at 447 $cm^{-1}$ was attributed to rutile phase. There were no significant differences between unmodified P25 and $TiO_2$ loaded with $WO_3$ from 0 to 5 mol%, but the new peaks can be observed especially at 273, 325, 714, 807 and 985 $cm^{-1}$ when $WO_3$ loading was beyond 5 mol%. The broad peak at 985 $cm^{-1}$ was detected at tungsten loading above 5 mol%, potentially due to the surface $WO_3$ species. Peak at 807 $cm^{-1}$ together with several other peaks at 273, 325, and 714 $cm^{-1}$ emerged at 12 mol% $WO_3$ loading, attributable to the crystalline $WO_3$ [28]. Sohn and Bae [31] have observed that when the tungsten loading is between 5 and 10 wt%, a broad and weak peak at ~935 $cm^{-1}$ appears. When loading is above 10 wt%, the peak shifts to ~968 $cm^{-1}$. The shift is possibly due to the tetrahedrally coordinated surface $WO_3$ in the former, and octahedrally coordinated polytungstate species in the latter. A broad band at 964 $cm^{-1}$ which is then shifted to wave number 980 $cm^{-1}$ when tungsten loading is increased, has also been reported [29]. This peak

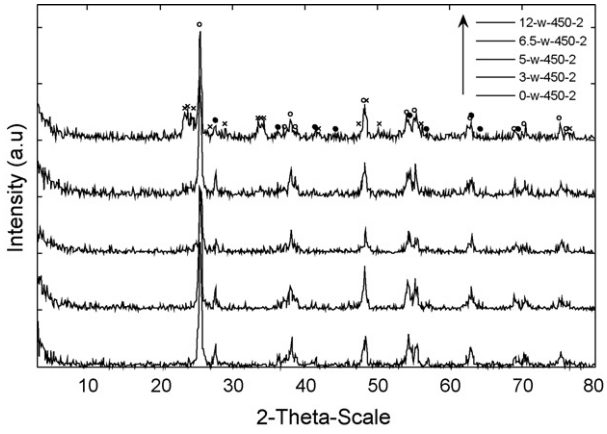


**Fig. 2.** X-ray diffractograms of $TiO_2$ with different tungsten loading (open circle = anatase, closed circle = rutile, cross = $WO_3$).

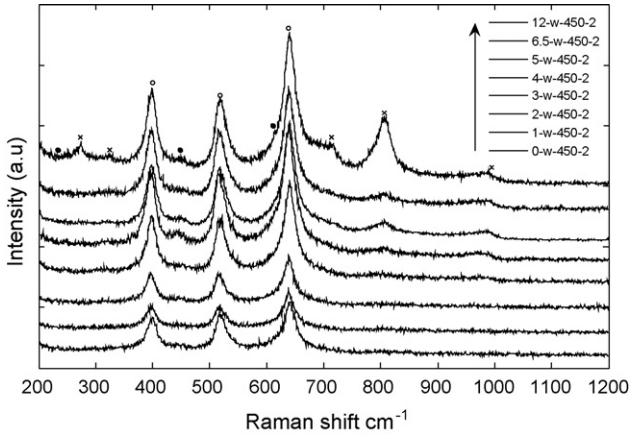


**Fig. 3.** Raman spectra of $TiO_2$ with different tungsten loading (open circle = anatase, closed circle = rutile, cross = $WO_3$).

is attributed to the W=O stretching mode of dispersed bidimensional tungsten oxide species on the surface of $TiO_2$ anatase. The wave numbers at which these are reported vary. Xu et al. [32] assign the symmetrical W=O stretching mode at around 970 $cm^{-1}$. Kim et al. [33] assign the value of 1010 $cm^{-1}$ when measured under dehydrated condition, as it is generally accepted that the terminal W=O of surface tungsten oxide species shift toward higher wave number upon dehydration [33]. The different values of W=O stretching could be a result of this degree of hydration.

The increased particle size may be caused by sintering (particles aggregation due to heat treatment) or the phase transition from the smaller anatase into bigger rutile size. In this study, sintering could not plausibly occur at this calcination temperature (450 °C) as bare $TiO_2$ did not show any sign of particle changes when compared to raw P25. Phase transition into rutile also may not take place as shown by XRD and Raman spectroscopy analysis (Figs. 2 and 3) where anatase phase remained stable. Similar observation has also been reported by Martín et al. [29]. The more agglomerated $WO_3$-loaded $TiO_2$ could be a result of the increasing surface hydrophilic property of $TiO_2$ due to the presence of $WO_3$ [34]. A more refined measurement using HRTEM has shown that lattice fringes of $WO_3/TiO_2$ at 3 mol% $WO_3$ loading are similar to those of pure $TiO_2$ with no $WO_3$ cluster found on the $TiO_2$ surface [35]. The surface of $TiO_2$ could have been covered with monolayer thickness at 3 mol% $WO_3$ loading. The agglomeration at tungsten loading higher than 3 mol% can be due to $WO_3$ covering $TiO_2$ in multiple layers and/or may act as "glues" that bind $TiO_2$ particles to form bigger agglomerates. This is further accentuated by higher calcinations temperatures as shown in Fig. 1.

The presence of $WO_3$ phase at higher loading suggests the formation of crystalline $WO_3$. Theoretically, it requires 3.2 mol% of $WO_3$ to cover the surface of P25 [35], with the dispersion capacity of $WO_3$ on anatase $TiO_2$ to be 4.85 $W^{6+}/nm^2$ of $TiO_2$ [32]. Depending on the preparation method, the formation of $WO_3$ microcrystal has been observed at W/Ti ratio ≥8% (ca. 7.4 mol% $WO_3$) [29], while others have reported no $WO_3$ phases up to 20 wt% [31]. Therefore, the importance of preparation method cannot be further emphasized. For example, whilst there is no peak of which could be ascribed to $W_xTi_{1-x}O_2$ on coupled $WO_3/TiO_2$ prepared by ball milling [36], studies on tungsten-doped $TiO_2$ prepared by sol gel method have shown the formation of new peaks associated with the solid solution of $W_xTi_{1-x}O_2$ [37,38]. It has been suggested that $TiO_2$ and $WO_3$ only form solid solution when it is calcined above ≥1000 °C [35]. Below this, $WO_3$ will not be doped into $TiO_2$ lattice but will spread on the surface of $TiO_2$. In our study, we postulate that the impregnation of $TiO_2$ with $WO_3$ with calcinations at 450 °C can only modify the surface of $TiO_2$.

### 3.1.2. Point zero of charge (PZC)

Surface charge of the oxide is a result of the acid-base equilibrium. It is a function of pH and ionic strength of the solution. Point zero of charge (PZC) is important characteristic of oxide in the solution which can give information on the surface charge [39]. PZC is defined as the pH of the medium at which the surface charge is zero and can be measured by using potentiometric titration at different ionic strength medium or mass titration method [26]. $TiO_2$ surface may have different ionization states depending on the pH of the suspension according to Eqs. (3) and (4):

$$TiOH + H^+ \Leftrightarrow TiOH_2^+ \quad (3)$$

$$TiOH + OH^- \Leftrightarrow TiO^- + H_2O \quad (4)$$

Fig. 4 shows the PZC curve for the synthesized photocatalyst based on mass titration. PZC was estimated by measuring pH at which further addition of solid catalyst did not change the pH of the suspension. If the pH of the suspension is lower than PZC, the surface charge is positive. On the other hand if the pH is higher than PZC, the surface charge is negative [26]. It can be seen that PZC values decreased with increasing tungsten loading up to 6.5 mol% $WO_3$ and the PZC value for 1-w-450-2 was 4.5. No appreciable changes were observed with further loading. Similar observation is also reported by Di Paola [40] with PZC as low as 2.8 for 5 mol% W. The pH for catalyst loading between 10 and 20% does not change appreciably and the PZC value can be estimated at this catalyst loading. The PZC value of $WO_3$ has been reported to be as low as 0.4 [39,41]. The PZC for P25 (0-w-450-2) was about 6.35, comparable to those reported in the literature for $TiO_2$ which is at 3.5–6.5 [39], though some have suggested the value of 7.1 [8,26,42]. The difference could be in the synthesis procedure as PZC value can be affected by heat treatment [39]. Loading of metal oxide onto the surface of $TiO_2$ can therefore remarkably change the PZC value. Certain metals such as Co, Cu, and Fe increase PZC value while metals such as Cr, Mo, V and W decrease PZC value [1,17,18]. The decreasing PZC value of tungsten-loaded $TiO_2$ is obviously due to the presence of $WO_3$.

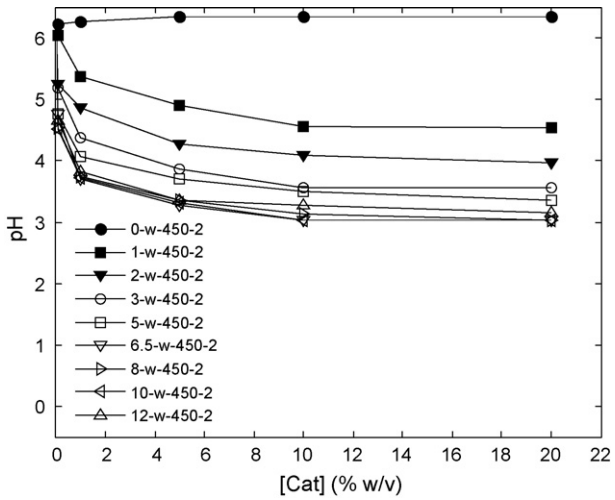


**Fig. 4.** Mass titration curves of $TiO_2$ with different tungsten loadings.

### 3.1.3. Absorption spectrum of $TiO_2$

One of the challenges in the development of $TiO_2$ is to shift the absorption spectrum of $TiO_2$ into the visible region to enable utilization of higher portion of sunlight. Fig. 5 shows the absorp-

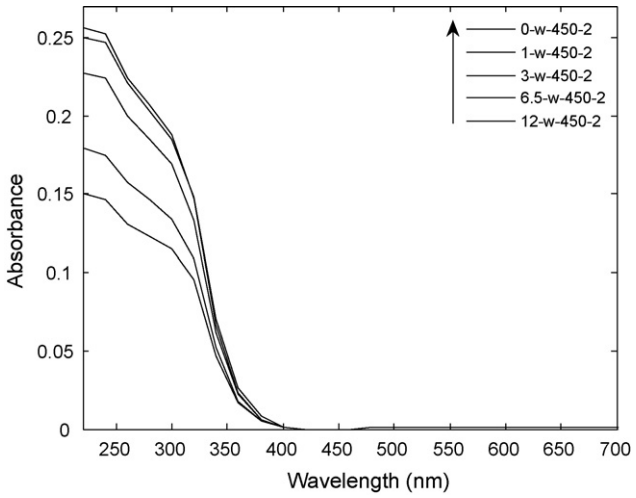


**Fig. 5.** Absorption spectrum of $TiO_2$ at different tungsten loadings.

tion spectrum of the synthesized photocatalyst. The absorption spectrum of $TiO_2$ was not much different from those loaded with 1 mol% of $WO_3$. However, further increases in metal loading decrease photon absorption. Others have reported a decrease in the photon absorption when $TiO_2$ loaded with 4 mol% of $WO_3$ [29]. Our study on modification of $TiO_2$ with $WO_3$ by using impregnation method has not shifted the absorption spectrum of $TiO_2$ into visible region. Similar results have been reported by Martín et al. [29] and Gutiérrez-Alejandre et al. [43]. The orbital 5d of W lies within the Ti 3d conduction band that the charge transfer of the $O^{2-} \rightarrow W^{6+}$ are likely to be mixed with the $O^{2-} \rightarrow Ti^{4+}$ [43].

Modification with metal can shift the absorption spectrum of $TiO_2$ into the visible region but this is very much dependent on the preparation method. Advanced metal ion implantation method for instance can shift the absorption spectrum of $TiO_2$ into the visible region, which is due to the incorporation of the metals (substitutionally or interstitially) into the lattice of $TiO_2$, thus modifying the electronic properties of bulk $TiO_2$ [44]. The shift in the absorption spectrum of $WO_3/TiO_2$ to the visible region has been observed when the photocatalysts were prepared using sol gel method [37,38]; ball milling method [36]; and hydrothermal method [45]. XPS analysis of 3 mol% $WO_3/TiO_2$ loading shows the existence of $W^{6+}$, $W^{5+}$, and $W^{4+}$ where the first two are predominant species. It is suggested that $W^{4+}$ can substitute $Ti^{4+}$ due to the similarity in ionic radius, forming the non-stoichiometric solid solution $W_xTi_{1-x}O_2$. Optical absorption measurement reveals that doping with tungsten shifts the absorption spectrum to the visible region, though no clear absorption edge is observed. In another study, the $WO_x$–$TiO_2$ prepared by sol mixing method shows the optimum tungsten loading at 1 mol% [38]. However, the XPS analysis of 1 mol% $WO_3/TiO_2$ similarly shows the existence of $W^{4+}$, $W^{5+}$, and $W^{6+}$, with the first two as predominant species, and the absorption spectrum of W-doped $TiO_2$ is found shifted to the visible light. Impregnation method can also shift the absorption spectrum of $TiO_2$ [8] where the shift is possibly caused by the impurity energy level within the bandgap of $TiO_2$ as the metal is spread on the surface, and not incorporated into $TiO_2$ framework. Nevertheless, bulk properties of $TiO_2$ are as important as surface properties of $TiO_2$ and should be considered in future effort to develop metal-doped $TiO_2$ photocatalyst activated in the visible region.

### 3.2. Photodegradation studies

#### 3.2.1. Effect of tungsten loadings

Fig. 6 shows photodegradation of MB as a function of tungsten loadings based on first-order kinetics. As a benchmark, the rate constant for unmodified $TiO_2$ was $16.1 \times 10^{-3}$ min$^{-1}$. The enhancement of photocatalytic activity ($k_1 = 16.5$–$28.0 \times 10^{-3}$ min$^{-1}$) occurred for 0.6–2 mol% $WO_3$ loading. At higher than 2 mol% $WO_3$, the photocatalytic activity decreased, while at lower than 0.6 mol% $WO_3$ loading, no significant enhancement in photocatalytic activity was observed. At 1 mol%, the rate constant was $28.0 \times 10^{-3}$ min$^{-1}$, approximately twice the rate constant of the unmodified $TiO_2$, while at 3 mol% $WO_3$, the rate constant was $11.2 \times 10^{-3}$ min$^{-1}$, lower than the unmodified $TiO_2$. The maximum improvement of MB degradation by flame-made $WO_3/TiO_2$ has been reported at 3.6 mol% [28], while others have reported only 40–50% increment at 3 mol% $WO_3/TiO_2$ [35]. However, the photocatalytic activity of $WO_3/TiO_2$ was maximized when the surface is covered with $WO_3$ with monolayer thickness, theoretically at 3.2 mol% $WO_3$, with the degradation of aqueous dichlorobenzene enhanced by 2.5-fold, and benzene and 2-propanol degradation in the gas phase enhanced by 3.6- and 5.9-fold, respectively [35]. The highest activity for $WO_x$–$TiO_2$ prepared using sol gel method for degradation of MB under visible lamp was at 3% $WO_3$ [37].

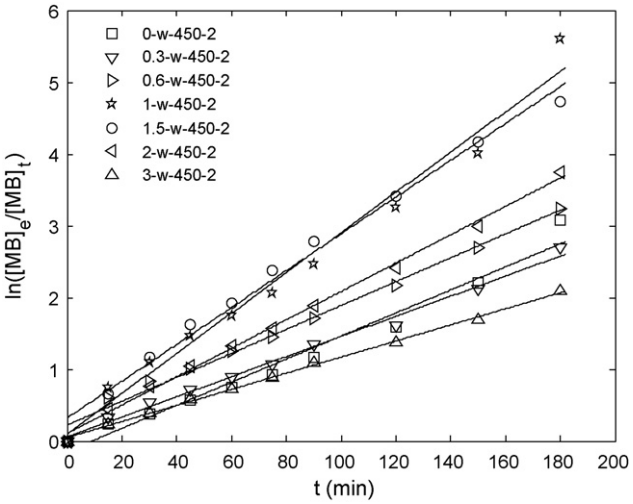


**Fig. 6.** Effect of tungsten loadings on methylene blue degradation.

#### 3.2.2. Effect of calcination temperatures

Calcination temperature and duration play important roles in shaping the characteristics and activities of the photocatalyst. To determine the optimum temperature, the catalyst was calcined at different calcination temperatures—450, 550, 650, 750 and 850 °C. Fig. 7 shows that with increasing temperatures, the anatase fraction of unmodified $TiO_2$ was decreasing rapidly from 650 °C onwards. The ratio of anatase fraction as calculated by using Eq. (1) for calcinations at 450 °C was 0.82, reduced to 0.71 at 550 °C and was significantly reduced to 0.06 at 650 °C. This may suggest that the phase transformation of anatase into rutile in unmodified $TiO_2$ occurred at 550–650 °C, which is comparable to the reported range at 500–600 °C [25]. The photocatalytic activity of unmodified $TiO_2$ decreased when calcined at 550 °C and reduced further when calcined at 650 °C or higher. Loading of tungsten into $TiO_2$ could potentially change the structural property of $TiO_2$. With tungsten loading at 1 mol%, the anatase fraction was still detectable for calcination temperature as high as 750 °C, and became negligible at 850 °C suggesting that the phase transformation could have occurred at 650–850 °C range which was broader and higher than the unmodified $TiO_2$. The photocatalytic activity remained high at 1 mol% of $WO_3$ for 550 °C calcination, and only slightly decreased at 650 °C, before being significantly reduced when calcined at 750 and 850 °C. At 6.5 mol% of $WO_3$, anatase was still the major phase for

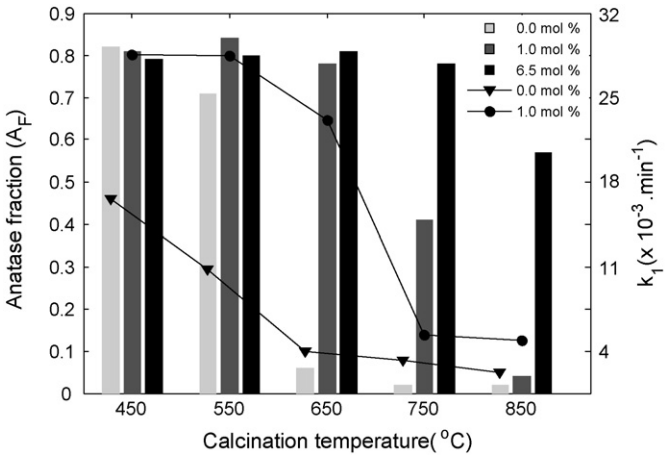


**Fig. 7.** Effect of tungsten loadings and calcination temperatures on anatase fraction and rate of MB photodegradation of unmodified $TiO_2$ (▼), and 1 mol% tungsten (●).

**Table 1**
Effects of different physical parameters on rate of MB degradation by 1-w-450-2.

| | $k_{app}$ ($\times 10^{-3}$ min$^{-1}$) | $r^2$ | SSE |
|---|---|---|---|
| A. [*MB*] initial (mg/L) | | | |
| 10 | 208 | 1.00 | 0.00 |
| 20 | 88 | 0.98 | 0.35 |
| 30 | 48 | 0.99 | 0.17 |
| 40 | 28 | 0.98 | 0.49 |
| 50 | 16 | 0.98 | 0.17 |
| 60 | 11 | 0.95 | 0.16 |
| B. [Cat] (g/L) | | | |
| 0.0 | 1 | 0.97 | 0.00 |
| 0.5 | 13 | 0.97 | 0.14 |
| 1.0 | 28 | 0.98 | 0.49 |
| 1.5 | 33 | 0.98 | 0.63 |
| 2.0 | 32 | 0.99 | 0.20 |
| C. pH | | | |
| 3.0 | 12 | 0.99 | 0.03 |
| 5.1 | 28 | 0.98 | 0.49 |
| 7.0 | 23 | 0.97 | 0.44 |
| 10.0 | 25 | 0.98 | 0.23 |

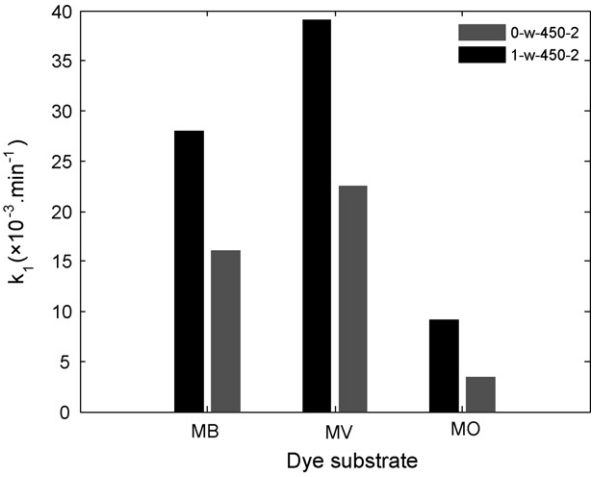


**Fig. 8.** Effect of dye substrates on the degradation rate constant.

calcinations as high as 850 °C. Further increase in tungsten loading apparently stabilized the anatase phase from transformation into inactive rutile, similar observation has also been made by others [38].

Phase transformation of anatase into rutile generally is unfavorable because it reduces the photocatalytic activity. Heat treatment however does not only affect $TiO_2$, but also $WO_3$. $WO_3$ has five different phases namely—α-$WO_3$ (tetragonal), β-$WO_3$ (orthorombic), γ-$WO_3$ (monoclinic), δ-$WO_3$ (triclinic), and ε-$WO_3$ (monoclinic) [46]. Upon heat treatment, these phases could have been transformed in the following order: ε-$WO_3$ (monoclinic, <−40 °C) → δ-$WO_3$ (triclinic, −40 to 17 °C) → γ-$WO_3$ (monoclinic, 17–320 °C) → β-$WO_3$ (orthorhombic, 320–720 °C) → α-$WO_3$ (tetragonal, >720 °C) [46]. The presence of $TiO_2$ can prevent the transformation of γ-$WO_3$ (monoclinic) into β-$WO_3$ (orthorhombic) [45,46]. The interaction of $TiO_2$ and $WO_3$ therefore not only prevents the transformation of the anatase phase into rutile phase, but also possibly the transformation of monoclinic phase of $WO_3$ into the orthorhombic phase.

### 3.2.3. *Effects of initial dye concentration, catalyst loading and initial pH*

The effects of initial dye concentration, catalyst loading and initial pH on the decolourization rate of MB by $TiO_2$ loaded with 1 mol% $WO_3$ are summarized in Table 1. The initial dye concentration must be determined for effective photocatalyst effects. The optimum photocatalyst loading can avoid utilization of excess catalyst and to ensure total absorption of photons, with maximum amount of photocatalyst achieving all surface totally illuminated. Rate of degradation is further affected by pH via change in ionization state of the photocatalyst surface and the substrate. As shown in Table 1, increasing the initial dye concentration from 10 to 60 mg/L reduced the rate of decolourization by almost 20-fold. Similar trend was reported for other dyes such as safira dye HEXL at 20–80 mg/L [47], acid red 14 at 20–40 mg/L [48], acid red 27 at 5–40 mg/L [49], metanil yellow at 40–100 mg/L [50], acid orange 20 at 25–100 mg/L [51], methyl orange at 5–75 mg/L [52]. At higher dye concentrations, degradation efficiency may decrease as the dye covered the active sites thus reducing the hydroxyl radical productions. In addition, there could also be the UV-screening effect of the dye where significant portion of UV light may be absorbed by the dyes rather than the photocatalyst [24].

Within the range of photocatalyst loading tested between 0 and 2 g/L, the amount of MB adsorbed onto 1-w-450-2 increased proportionally with the loadings. MB decolourization rate increased with increasing photocatalyst loadings up to 1 g/L, and further increase did not significantly increase the rate of decolourization whilst the rate becoming independent of the effect of photocatalyst loadings. Degradation of methyl orange by complex nanoparticle $WO_3/TiO_2$ reaches optimum conditions at 8 g/L photocatalyst loading [53]. However, when tested using $SO_4^{2-}/TiO_2$ system, the rate increases with increasing photocatalyst concentration up to 2 g/L before it reaches saturation.

As stated earlier, the unmodified $TiO_2$ in our study had PZC value of 6.4. This was close to neutral pH and $TiO_2$ surface was therefore negatively charged under basic condition but positively charged under acidic condition. For 1-w-450-2 where the PZC value was 4.5, it was negatively charged at pH higher than 4.5 and positively charged at pH lower than 4.5. From Table 1, the pH condition was chosen at 3, 7, and 10 to simulate the acidic, neutral and basic condition. The rate was also evaluated at pH 5.1 without adjustment. It can be observed that increase in pH had resulted in higher MB adsorption. Decolourization rate of MB was highest ($k_{app} = 28 \times 10^{-3}$ min$^{-1}$) at pH 5.1 without adjustment. At pH 3, the rate of decolourization was significantly decreased ($k_{app} = 12 \times 10^{-3}$ min$^{-1}$). Increasing pH to neutral pH and further to pH 10 only slightly reduced the rate of decolourization rate ($k_1 = 23–25 \times 10^{-3}$ min$^{-1}$). Considering the PZC value of 4.5, the higher adsorption of MB at higher pH can be attributed to the coulombic interaction of the negatively charged 1-w-450-2 surfaces with the positively charged MB molecules. $TiO_2$ tends to agglomerate under acidic condition and therefore the surface area available for dye adsorption and photon absorption will be reduced [24]. At basic pH, there is higher affinity towards MB due to coulombic interaction and also higher production of hydroxyl radicals from the reaction of hydroxide ions with the positive holes [24].

### 3.2.4. *Effect of dye substrates*

The photocatalytic activity of 1-w-450-2 was tested against other types of dyes such as methyl violet (MV) and methyl orange (MO) in addition to MB. MV is a cationic dye of the triarylmethane class, while MO is an anionic dye of azo dye class and MB is a cationic dye of thiazine class. Comparison on the decolourization rate constant of MB, MV and MO is depicted in Fig. 8. Similar to MB, the degradation of both dyes followed first-order kinetics with coefficient of determination ($r^2$) ranging from 0.93 to 0.99 and sum of squared errors (SSEs) from 0.00 to 0.42. Using unmodified $TiO_2$, the decolourization rate of MV ($k_1 = 22.6 \times 10^{-3}$ min$^{-1}$) was higher than MB ($k_1 = 16.1 \times 10^{-3}$ min$^{-1}$), while MO ($k_1 = 3.4 \times 10^{-3}$ min$^{-1}$) was slower to degrade. The type of dyes therefore greatly affects

the rate of decolourization. Nevertheless, the degradation rate of all dyes by 1-w-450-2 was higher than the unmodified $TiO_2$. MV and crystal violet (CV) has similar chemical structure, the difference being only in the degree of N-methylation. Couselo et al. [54] report that the decolourizaton mechanism of crystal violet by tungsten-doped $TiO_2$ is different from pure $TiO_2$. The mechanism in the former follows the rupture of aromatic ring mechanism rather than N-demethylation mechanism which is more prone to occur in pure $TiO_2$. Although 1 mol% $WO_3$ is the optimum tungsten loading for MB degradation, the optimum tungsten loading for degradation of other dyes could be different. The optimum tungsten loading for the degradation of CV has been reported within the range of 2–5 mol% W [54] and at 3 wt% for MO [53].

## 4. Conclusions

The tungsten-loaded $TiO_2$ photocatalyst has been successfully synthesized and characterized. Tungsten–$TiO_2$ interaction stabilized the active anatase phase from transforming into inactive rutile phase and γ-$WO_3$ into β-$WO_3$. The higher the tungsten loading, the more stable the photocatalyst became, as compared to the unmodified $TiO_2$. However, the impregnation method used in the synthesis did not shift the optical absorption to the visible region. Optimum degradation of MB was achieved at dilute dye concentration ($\leq$10 mg/L), catalyst loading of 1 g/L and pH without adjustment of 5.1. The photocatalyst can withstand neutral to alkaline condition of up to pH 10, but showed poor performance in condition, pH 3. The photocatalyst was also effective for degradation of different class of dyes such as methyl violet and methyl orange. For highly concentrated wastewater, dilution and pH adjustment may be crucial step prior to photocatalytic treatments.

## Acknowledgements

The authors would like to thank Universiti Teknologi Petronas for the scholarship to Saepurahman and for the research facilities. The STIRF Grant no. 10/06.07 that funded this project is highly acknowledged.

## References

[1] Y. Anjaneyulu, N. Sreedhara Chary, D. Samuel Suman Raj, Decolourization of industrial effluents—available methods and emerging technologies—a review, Rev. Environ. Sci. Biotechnol. 4 (2005) 245–273.
[2] C. Binnie, M. Kimber, G. Smethurst, Basic Water Treatment, third ed., Royal Society of Chemistry, London, 2002.
[3] J.H. Clark, D. Macquarrie, Handbook of Green Chemistry and Technology, Blackwell Publishing, Oxford, 2002.
[4] M.R. Hoffmann, S.T. Martin, W. Choi, D.W. Bahnemann, Environmental applications of semiconductor photocatalysis, Chem. Rev. 95 (1995) 69–96.
[5] N.S. Lewis, Light work with water, Nature 414 (2001) 589–590.
[6] Y. Bessekhouad, D. Robert, J.V. Weber, N. Chaoui, Effect of alkaline-doped $TiO_2$ on photocatalytic efficiency, J. Photochem. Photobiolol. A 167 (2004) 49–57.
[7] N. Venkatachalam, M. Palanichamy, V. Murugesan, Sol–gel preparation and characterization of alkaline earth metal doped nano-$TiO_2$: efficient photocatalytic degradation of 4-chlorophenol, J. Mol. Catal. A: Chem. 273 (2007) 177–185.
[8] A. Di Paola, G. Marci, L. Palmisano, M. Schiavello, K. Uosaki, S. Ikeda, B. Ohtani, Preparation of polycrystalline $TiO_2$ photocatalysts impregnated with various transition metal ions: characterization and photocatalytic activity for the degradation of 4-nitrophenol, J. Phys. Chem. B 106 (2002) 637–645.
[9] A.W. Xu, Y. Gao, H.Q. Liu, The preparation, characterization, and their photocatalytic activities of rare-earth-doped $TiO_2$ nanoparticles, J. Catal. 207 (2002) 151–157.
[10] J.C. Colmenares, M.A. Aramendía, A. Marinas, J.M. Marinas, F.J. Urbano, Synthesis, characterization and photocatalytic activity of different metal-doped titania systems, Appl. Catal. A 306 (2006) 120–127.
[11] S. Riyas, V.A. Yasir, P.N. Mohan Das, Crystal structure transformation of $TiO_2$ in presence of $Fe_2O_3$ and NiO in air atmosphere, Bull. Mater. Sci. 25 (2002) 267–273.
[12] G. Sankar, K. Kannan, C. Rao, Anatase–rutile transformation in Fe/$TiO_2$, Th/$TiO_2$ and Cu/$TiO_2$ catalysts and its possible role in metal–support interaction, Catal. Lett. 8 (1991) 27–36.
[13] B.M. Reddy, E.P. Reddy, S. Mehdi, Phase transformation study of titania in $V_2O_5$/$TiO_2$ and $MoO_3$/$TiO_2$ catalysts by X-ray diffraction analysis, Mater. Chem. Phys. 36 (1994) 276–281.
[14] M. Barakat, G. Hayes, S. Shah, Effect of cobalt doping on the phase transformation of $TiO_2$ nanoparticles, J. Nanosci. Nanotechnol. 5 (2005) 759–765.
[15] S. Mahanty, S. Roy, S. Sen, Effect of Sn doping on the structural and optical properties of sol–gel $TiO_2$ thin films, J. Cryst. Growth 261 (2004) 77–81.
[16] S. Sen, S. Mahanty, S. Roy, O. Heintz, S. Bourgeois, D. Chaumont, Investigation on sol–gel synthesized Ag-doped $TiO_2$ cermet thin films, Thin Solid Films 474 (2005) 245–249.
[17] N. Venkatachalam, M. Palanichamy, B. Arabindoo, V. Murugesan, Alkaline earth metal doped nanoporous $TiO_2$ for enhanced photocatalytic mineralisation of bisphenol-A, Catal. Commun. 8 (2007) 1088–1093.
[18] R. Arroyo, G. Cordoba, J. Padilla, V. Lara, Influence of manganese ions on the anatase-rutile phase transition of $TiO_2$ prepared by the sol–gel process, Mater. Lett. 54 (2002) 397–402.
[19] M. Saif, M.S.A. Abdel-Mottaleb, Titanium dioxide nanomaterial doped with trivalent lanthanide ions of Tb, Eu and Sm: preparation, characterization and potential applications, Inorg. Chim. Acta 360 (2007) 2863–2874.
[20] K.M. Parida, N. Sahu, Visible light induced photocatalytic activity of rare earth titania nanocomposites, J. Mol. Catal. A: Chem. 287 (2008) 149–156.
[21] A. Ahmad, S. Buzby, C. Ni, S.I. Shah, Effect of Nb and Sc doping on the phase transformation of sol–gel processed $TiO_2$ nanoparticles, J. Nanosci. Nanotechnol. 8 (2008) 2410–2418.
[22] J.M. Herrmann, Heterogeneous photocatalysis: fundamentals and applications to the removal of various types of aqueous pollutants, Catal. Today 53 (1999) 115–129.
[23] D. Beydoun, Development of a novel magnetic photocatalyst: preparation, characterization and implication for organic degradation in aqueous systems, School of Chemical Engineering and Industrial Chemistry, The University of New South Wales. PhD thesis (2000).
[24] I.K. Konstantinou, T.A. Albanis, $TiO_2$-assisted photocatalytic degradation of azo dyes in aqueous solution: kinetic and mechanistic investigations: a review, Appl. Catal. B 49 (2004) 1–14.
[25] N.R.C. Fernandes Machado, V.S. Santana, Influence of thermal treatment on the structure and photocatalytic activity of $TiO_2$ P25, Catal. Today 107 (2005) 595–601.
[26] A. Di Paola, E. García-López, G. Marcì, C. Martín, L. Palmisano, V. Rives, A. Maria Venezia, Surface characterisation of metal ions loaded $TiO_2$ photocatalysts: structure–activity relationship, Appl. Catal. B 48 (2004) 223–233.
[27] G.J. French, F.R. Sale, A re-investigation of the thermal decomposition of ammonium paratungstate, J. Mater. Sci. 16 (1981) 3427–3436.
[28] K.K. Akurati, A. Vital, J.-P. Dellemann, K. Michalow, T. Graule, D. Ferri, A. Baiker, Flame-made $WO_3$/$TiO_2$ nanoparticles: relation between surface acidity, structure and photocatalytic activity, Appl. Catal. B 79 (2008) 53–62.
[29] C. Martín, G. Solana, V. Rives, G. Marcì, L. Palmisano, A. Sclafani, Physicochemical properties of $WO_3$/$TiO_2$ systems employed for 4-nitrophenol photodegradation in aqueous medium, Catal. Lett. 49 (1997) 235–243.
[30] X. Chen, S.S. Mao, Titanium dioxide nanomaterials: synthesis, properties, modifications, and applications, Chem. Rev. 107 (2007) 2891–2959.
[31] J. Sohn, J. Bae, Characterization of tungsten oxide supported on $TiO_2$ and activity for acid catalysis, Korean J. Chem. Eng. 17 (2000) 86–92.
[32] B. Xu, L. Dong, Y. Fan, Y. Chen, A study on the dispersion of NiO and/or $WO_3$ on anatase, J. Catal. 193 (2000) 88–95.
[33] D.S. Kim, M. Ostromecki, I.E. Wachs, Surface structures of supported tungsten oxide catalysts under dehydrated conditions, J. Mol. Catal. A: Chem. 106 (1996) 93–102.
[34] H. Irie, H. Mori, K. Hashimoto, Interfacial structure dependence of layered $TiO_2$/$WO_3$ thin films on the photoinduced hydrophilic property, Vacuum 74 (2004) 625–629.
[35] Y. Tae Kwon, K. Yong Song, W. In Lee, G. Jin Choi, Y. Rag Do, Photocatalytic behavior of $WO_3$-loaded $TiO_2$ in an oxidation reaction, J. Catal. 191 (2000) 192–199.
[36] C. Shifu, C. Lei, G. Shen, C. Gengyu, The preparation of coupled $WO_3$/$TiO_2$ photocatalyst by ball milling, Powder Technol. 160 (2005) 198–202.
[37] X.Z. Li, F.B. Li, C.L. Yang, W.K. Ge, Photocatalytic activity of $WO_x$–$TiO_2$ under visible light irradiation, J. Photochem. Photobiol. A 141 (2001) 209–217.
[38] H. Song, H. Jiang, X. Liu, G. Meng, Efficient degradation of organic pollutant with $WO_x$ modified nano-$TiO_2$ under visible irradiation, J. Photochem. Photobiol. A 181 (2006) 421–428.
[39] J.P. Jolivet, M. Henry, J. Livage, Metal Oxide Chemistry and Synthesis, Wiley, New York, 2000.
[40] A. Di Paola, Transition metal doped $TiO_2$: physical properties and photocatalytic behaviour, Int. J. Photoenergy 3 (2001) 171–176.
[41] Y. Xu, M.A.A. Schoonen, The absolute energy positions of conduction and valence bands of selected semiconducting minerals, Am. Mineral 85 (2000) 543–556.
[42] A. Di Paola, E. Garcïía-López, S. Ikeda, G. Marci, B. Ohtani, L. Palmisano, Photocatalytic degradation of organic compounds in aqueous systems by transition metal doped polycrystalline $TiO_2$, Catal. Today 75 (2002) 87–93.
[43] A. Gutiérrez-Alejandre, J. Ramírez, G. Busca, The electronic structure of oxide-supported tungsten oxide catalysts as studied by UV spectroscopy, Catal. Lett. 56 (1998) 29–33.
[44] M. Anpo, M. Takeuchi, The design and development of highly reactive titanium oxide photocatalysts operating under visible light irradiation, J. Catal. 216 (2003) 505–516.

[45] D. Ke, H. Liu, T. Peng, X. Liu, K. Dai, Preparation and photocatalytic activity of $WO_3/TiO_2$ nanocomposite particles, Mater. Lett. 62 (2008) 447–450.
[46] Z. Pintér, Z. Sassi, S. Kornely, C. Pion, I.V. Perczel, K. Kovács, R. Bene, J.C. Bureau, F. Réti, Thermal behaviour of $WO_3$ and $WO_3/TiO_2$ materials, Thin Solid Films 391 (2001) 243–246.
[47] T. Sauer, G. Cesconeto Neto, H.J. José, R. Moreira, Kinetics of photocatalytic degradation of reactive dyes in a $TiO_2$ slurry reactor, J. Photochem. Photobiol. 149 (2002) 147–154.
[48] N. Daneshvar, D. Salari, A.R. Khataee, Photocatalytic degradation of azo dye acid red 14 in water: investigation of the effect of operational parameters, J. Photochem. Photobiol. A 157 (2003) 111–116.
[49] M.N. Behnajady, Nonlinear regression analysis of kinetics of the photocatalytic decolorization of an azo dye in aqueous $TiO_2$ slurry, Photochem. Photobiol. Sci. 5 (2006) 1078–1081.
[50] M. Sleiman, D. Vildozo, C. Ferronato, J.M. Chovelon, Photocatalytic degradation of azo dye Metanil Yellow: optimization and kinetic modeling using a chemometric approach, Appl. Catal. B 77 (2007) 1–11.
[51] T. Papadam, N.P. Xekoukoulotakis, I. Poulios, D. Mantzavinos, Photocatalytic transformation of acid orange 20 and Cr (VI) in aqueous $TiO_2$ suspensions, J. Photochem. Photobiol. A 186 (2007) 308–315.
[52] N. Guettaï, H. Ait Amar, Photocatalytic oxidation of methyl orange in presence of titanium dioxide in aqueous suspension. Part I: Parametric study, Desalination 185 (2005) 427–437.
[53] Y. Cui, Photocatalytic degradation of MO by complex nanometer particles $WO_3/TiO_2$, Rare Met. 25 (2006) 649–653.
[54] N. Couselo, F.S. GarciaEinschlag, R.J. Candal, M. Jobbagy, Tungsten-doped $TiO_2$ vs. pure $TiO_2$ photocatalysts: effects on photobleaching kinetics and mechanism, J. Phys. Chem. C 112 (2008) 1094–1100.